Journal Pre-proof

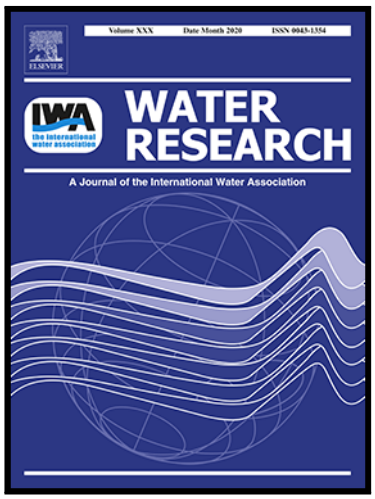

Mapping particulate organic carbon in lakes across China using OLCI/Sentinel-3 imagery

Dong Liu , Shujie Yu , Harriet Wilson , Kun Shi , Tianci Qi , Wenlei Luo , Mengwei Duan , Zhiqiang Qiu , Hongtao Duan

PII: S0043-1354(23)01474-4
DOI: https://doi.org/10.1016/j.watres.2023.121034
Reference: WR 121034

To appear in: *Water Research*

Received date: 3 October 2023
Revised date: 6 December 2023
Accepted date: 18 December 2023

Please cite this article as: Dong Liu , Shujie Yu , Harriet Wilson , Kun Shi , Tianci Qi , Wenlei Luo , Mengwei Duan , Zhiqiang Qiu , Hongtao Duan , Mapping particulate organic carbon in lakes across China using OLCI/Sentinel-3 imagery, *Water Research* (2023), doi: https://doi.org/10.1016/j.watres.2023.121034

Highlights

- A novel blended algorithm was proposed to remotely observe lake POC across China.
- POC concentrations in 450 large lakes were first mapped using OLCI/Sentinel-3 data.
- Lake POC concentration across China was low in the west and high in the east.

Mapping particulate organic carbon in lakes across China using OLCI/Sentinel-3 imagery

Dong Liu[a,b,#], Shujie Yu[c,#], Harriet Wilson[b], Kun Shi[d,*], Tianci Qi[a], Wenlei Luo[d,e], Mengwei Duan[a], Zhiqiang Qiu[a], Hongtao Duan[a,*]

[a] Key Laboratory of Watershed Geographic Sciences, Nanjing Institute of Geography and Limnology, Chinese Academy of Sciences, Nanjing 210008, China

[b] School of Biological and Environmental Science, University of Stirling, Stirling FK9 4LA, United Kingdom

[c] State Key Laboratory of Satellite Ocean Environment Dynamics, Second Institute of Oceanography, Ministry of Natural Resources, Hangzhou, 310012, China

[d] Taihu Laboratory for Lake Ecosystem Research, State Key Laboratory of Lake Science and Environment, Nanjing Institute of Geography and Limnology, Chinese Academy of Sciences, Nanjing 210008, China

[e] The Fuxianhu Station of Plateau Deep Lake Field Scientific Observation and Research, Yunnan, Yuxi 653100, China

* Corresponding author. *E-mail address*: kshi@niglas.ac.cn (K. Shi); htduan@niglas.ac.cn (H. Duan)

[#] Dong Liu and Shujie Yu contributed equally to this manuscript.

Abstract: Remote sensing monitoring of particulate organic carbon (POC) concentration is essential for understanding phytoplankton productivity, carbon storage, and water quality in global lakes. Some algorithms have been proposed, but only for regional eutrophic lakes. Based on *in-situ* data (N = 1269) in 49 lakes across China, we developed a blended POC algorithm by distinguishing Type-I and Type-II waters. Compared to Type-I, Type-II waters had higher reflectance peak around 560 nm (> 0.0125 sr^{-1}) and mean POC (4.65 ± 4.11 vs. 2.66 ± 3.37 mg/L). Furthermore, because POC was highly related to algal production (r = 0.85), a three-band index (R^2 = 0.65) and the phytoplankton fluorescence peak height (R^2 = 0.63) were adopted to estimate POC in Type-I and Type-II waters, respectively. The novel algorithm got a mean absolute percent difference (MAPD) of 35.93% and outperformed three state-of-the-art formulas with MAPD values of 40.56 – 76.42%. Then, the novel algorithm was applied to OLCI/Sentinel-3 imagery, and we first obtained a national map of POC in 450 Chinese lakes (> 20 km^2), which presented an apparent spatial pattern of "low in the west and high in the east". In brief, water classification should be considered when remotely monitoring lake POC concentration over a large area. Moreover, a process-oriented method is required when calculating water column POC storage from satellite-derived POC concentrations in type-II waters. Our results contribute substantially to advancing the dynamic observation of the lake carbon cycle using satellite data.

Keywords: particulate organic carbon; bio-optical properties; inland lakes; remote sensing; OLCI/Sentinel-3 imagery

1 Introduction

Lakes regulate the global carbon cycle by receiving a large amount of carbon from the terrestrial ecosystems (Drake et al., 2017; Regnier et al., 2022), emitting greenhouse gases (0.32 Pg C/yr of carbon dioxide (CO_2) and 0.10 Pg C/yr of methane (CH_4) into the atmosphere (Bastviken et al., 2011; Raymond et al., 2013), outputting carbon (0.9 Pg C/yr) into the oceans (Tranvik et al., 2009), and storing carbon (not known) as various forms in water columns (Mendonca et al., 2017; Tranvik et al., 2009). Of the reserved carbon, particulate organic carbon (POC) refers to the organic carbon contained in suspended sediment, phytoplankton, bacteria, and excrement, which provide food/energy for microbial metabolism and consume dissolved oxygen via aerobic degradation (Artifon et al., 2019; Xu et al., 2021). Moreover, POC concentration spatiotemporally varies across different lakes, eutrophication levels, and hydrological conditions (Liu et al., 2023; Wang et al., 2021). Therefore, to better understand the lake carbon cycle and water quality, it is important to dynamically monitor lake POC using widely covered and periodically revisited satellite data.

Because POC itself is not light-sensitive, remote sensing algorithms for POC are primarily determined by the host composition (Jiang et al., 2019; Son et al., 2009; Stramska, 2005). For the ocean, where POC is mainly produced by phytoplankton, POC remote sensing technology has been well-developed since the 1990s, and the algorithms fall into three types (Brewin et al., 2023; Stramska, 2005; Stramski et al., 1999). Type I directly estimates POC from band reflectance through empirical

equations (Le et al., 2018; Stramski et al., 2022). Type II first derives chlorophyll-a (Chl-a) concentration from satellite reflectance and then calculates POC from Chl-a (Stramska, 2005). Type III calculates POC based on inherent optical properties (backscattering, attenuation, or absorption coefficients), which are priorly remotely derived through semi-analytic algorithms (Stramska, 2005; Stramski et al., 1999).

Following the above three types, some algorithms have been proposed to remotely derive lake POC concentrations over the past decade. Compared to the ocean, lake POC is sourced from both algae production and sediment resuspension, both of which show high spatiotemporal variations (Liu et al., 2023; Wang et al., 2021; Xu et al., 2021). However, all previous studies focused on turbid eutrophic lakes located along the Yangtze River, China (Huang et al., 2019; Jiang et al., 2019; Lin et al., 2018; Liu et al., 2023; Xu et al., 2021). The results indicated that the bio-optical properties of POC differ within intra- / inter-lake and water classification is priorly required to realize the remote sensing monitoring of POC in different lakes (Jiang et al., 2019; Liu et al., 2023; Xu et al., 2021). In general, lake waters are first identified as the phytoplankton- or sediment-dominated POC types, and then two kinds of bio-optical equations are respectively developed to derive POC (Jiang et al., 2019; Lin et al., 2018).

Except for shallow turbid eutrophic lakes, 67% of the global lake area is characterized by deep water depth (≥ 6 m), low algae production, and high transparency (Hou et al., 2022; Messager et al., 2016; Song et al., 2022). In contrast to turbid eutrophic lakes, clear lakes usually have lower water reflectance and

Chl-a fluorescence peaks around 700 nm (Spyrakos et al., 2018); POC in clear lakes is less contributed by sediment resuspension (Jiang et al., 2019); moreover, clear lakes commonly have higher ratios of POC to Chl-a (POC:Chl-a) (Liu et al., 2023). In these cases, we believe previous POC algorithms for turbid lakes are not applicable to clear lakes (Jiang et al., 2019; Le et al., 2018); namely, we need to further develop a blended remote sensing algorithm to monitor POC concentrations across shallow-to-deep, turbid-to-clear, and oligotrophic-to-eutrophic lakes. Actually, the water classification method has also been recommended for remotely observing Chl-a (Liu et al., 2021) and total suspended matter (TSM) (Jiang et al., 2021) across global lakes. Moreover, the classification strategies are based on the bio-optical properties of the concerned variables (Jiang et al., 2021; Lin et al., 2018; Liu et al., 2021).

Using *in-situ* bio-optical data in 49 lakes (N = 1269) across China, this study developed a novel blended algorithm for synchronously monitoring POC concentrations in different lake types. The algorithm was then applied to the advanced data acquired by the Ocean and Land Colour Instrument onboard the Sentinel-3 satellite (OLCI/Sentinel-3) to derive POC in 450 Chinese lakes (> 20 km^2). Results were analyzed in regard to the spatial variations in lake POC across China, and the implications for water column-integrated POC storage estimation were discussed. This study is of great significance for developing POC remote sensing technology and better understanding the global lake carbon cycle.

2 Study area

In China, there are 2693 natural lakes with an area of > 1 km^2 (Fig. 1), which are mainly concentrated in the western Tibet Plateau and the eastern Yangtze-Huai Plain (Liu et al., 2023; NIGLAS, 2019). Overall, the western lakes generally have higher elevation, lower precipitation, lower turbidity, and lower eutrophication levels than the eastern lakes (Hou et al., 2022; Liu et al., 2020; Messager et al., 2016). According to the topography, precipitation, and province boundaries, previous studies defined five geographic lake zones (Ma et al., 2010; NIGLAS, 2019): the Inner Mongolia-Xinjiang Lake zone (IMXL), the Tibetan Plateau Lake zone (TPL), the Yunan-Guizhou Plateau Lake zone (YGPL), the Northeast Plain and Mountain Lake zone (NPML), and the Eastern Plain Lake zone (EPL) (Fig. 1).

This study focuses on 450 Chinese lakes (> 20 km^2), which are discernible from the OLCI/Sentinel-3 data with a spatial resolution of 300 m (Jiang et al., 2021; Lin et al., 2018) and have available remote sensing Chl-a and TSM products from the European Space Agency (Section 3.4). The studied lakes have a total water area of 74,343 km^2, which accounts for 91.31% of all Chinese lakes (Ma et al., 2010). Among them, 52, 274, 10, 26, and 88 lakes are distributed in the IMXL, TPL, YGPL, NPML, and EPL zones, respectively (Fig. 1). It should be noted that the entire lake bodies of the transnational Bangong (TPL), BuirNur, and Xingkai (NPML) were considered when calculating lake-based mean POC concentrations.

3 Materials and methods

3.1 Field sampling and measurements

For the studied lakes, 45 cruises were conducted to investigate the bio-optical properties of lake waters during 2011-2022 (Supplementary Table S1). Specifically, *in-situ* bio-optical data at 1269 stations were collected from 49 lakes, with 9, 19, 1, 1, and 18 in the IMXL, TPL, YGPL, NPML, and EPL zones, respectively (Table 1, Fig. 1). In addition, profile sampling for POC concentration was also done in Lake Fuxian in 2022 (N = 12) and Lake Chaohu in 2017 (N = 50) (Table S2). For the deep Lake Fuxian (NIGLAS, 2019), the sampling depths were 0, 10, 20, 30, 40, 50, 60, 100, 120, and 150 m. For the shallow Lake Chaohu, the sampling depths were 0, 10, 20, 40, 70, 100, 150, 200, and 300 m (Liu et al., 2023).

At each field station, raw water was sampled using a brown high-density polyethylene bottle and refrigerated at 4°C; conductivity was measured using a *YSI* multi-parameter meter (www.ysi.com); transparency was determined by the visible Secchi-disk depth (SDD) (Liu et al., 2020; Mueller et al., 2003); and radiance spectra of water (L_w), skylight (L_{sky}), and a grey diffuse reflectance standard plate (L_p) within 350-2390 nm with an interval of 1 nm were recorded using an *ASD* FieldSpec Spectroradiometer by following the NASA protocol (Mueller et al., 2003). Then, the field remote sensing reflectance (R_{field}) was calculated via Eq. (1).

$$R_{field} = (L_w - r \cdot L_{sky}) / (\pi \cdot L_p / \rho) \quad (1)$$

where ρ is the reflectance of the standard plate; r indicates the air-water interface reflectance and is calculated using the HydroLight platform (Mobley, 1999).

3.2 Lab analysis of biochemical parameters

After field investigation, raw waters were immediately filtrated through *Whatman* GF/F filters (0.7 μm pore size) to obtain POC and Chl-a samples within four hours. The filters for collecting POC had been pre-combusted at 450°C for six hours (Knap et al., 1996). Then, all samples were kept frozen at -18°C until lab analysis. In the Lab, POC samples were fumigated using 90% HCl to remove inorganic carbon (12 h), dried in an oven (105°C, 4 h), weighed (± 0.1 mg), and measured through the high-temperature combustion method using a *Euro Vector* EA3000 analyzer (Knap et al., 1996; Liu et al., 2023). Chl-a samples were extracted using 90% ethanol (10 mL, 24 h), heated in a thermostatic water bath (85°C, 3 – 5 min), and determined by a *Shimadzu* UV2401 spectrophotometer (Knap et al., 1996). Finally, *in-situ* POC and Chl-a concentrations were calculated using Eq. (2):

$$\begin{aligned} \text{POC} &= (W \cdot P) \ / \ V_1 \\ \text{Chl-a} &= (116.4 \cdot (A_{663} - A_{750}) - 21.6 \cdot (A_{645} - A_{750}) \\ &\quad + 1.0 \cdot (A_{630} - A_{750}))/V_2 \end{aligned} \tag{2}$$

where V_1 and V_2 are the filtration volumes of raw waters for POC and Chl-a samples, respectively; W denotes the total dry weight of the POC sample; P indicates the carbon mass percent of the POC sample; A_{630}, A_{645}, A_{663}, and A_{750} are the light absorbance of the ethanol extract of Chl-a at 630, 645, 663, and 750 nm.

3.3 OLCI/Sentinel-3 imagery

OLCI instruments, carried by the Sentinel-3A and -3B satellites, have spatiotemporal coverage advantages (300 m, ~1.5 days) for observing lakes and will provide consecutive data in the following 20-30 years along with the future

launches of the Sentinel-3C and -3D satellites (Doerffer, 2010; Liu et al., 2023). Therefore, OLCI/Sentinel-3 data were adopted to retrieve POC concentrations in the 450 studied lakes (Fig. 1). To be specific, we first downloaded daily OLCI/Sentinel-3A data (Level-1B) acquired in July 2017 from the Copernicus Open Access Hub (https://scihub.copernicus.eu/), then atmospherically corrected them to obtain water reflectance using the C2RCC processor in SNAP platform (Brockmann et al., 2016; Doerffer, 2010), and finally geographically clipped according to the lake boundaries from the National Earth System Science Data Center (http://lake.geodata.cn/). C2RCC could get good results for Case-II lake waters, which has been validated in various studies (Brockmann et al., 2016). Then, the output water reflectance was applied to further estimate POC using the calibrated algorithms (Section 4).

3.4 Multi-source product datasets

Except for POC, the corrected OLCI/Sentinel-3 band reflectance was also used to calculate the absorption coefficient of phytoplankton pigment ($a_{pig}(443)$, m^{-1}) and the backscattering coefficient of TSM ($b_{TSM}(443)$, m^{-1}) at 443 nm through an inverse neural network system in SNAP platform (Doerffer, 2010). Then, Chl-a and TSM contents were calculated using $a_{pig}(443)$ and $b_{TSM}(443)$, respectively (Eq. (3)):

$$\begin{aligned} [\text{Chl-a}] &= 22 \times a_{pig}(443)^{1.04} \\ [\text{TSM}] &= 1.7 \times b_{TSM}(443) \end{aligned} \tag{3}$$

where [Chl-a] and [TSM] indicate Chl-a and TSM concentrations, respectively. Eq. (3) denotes the recommended algorithms to derive Chl-a and TSM in global lakes

from OLCI/Sentinel-3 imagery with satisfactory results (Doerffer, 2010).

In addition, depth, elevation, and population data were also used to describe the spatial variations in lakes' POC concentrations. Lake depth and elevation were obtained from the HydroLAKES dataset (Messager et al., 2016). Km-grid population density data in 2015, sourced from the Resource and Environment Science and Data Center (https://www.resdc.cn/), were adopted to calculate the mean value of each lake watershed. As shown in supplementary Fig. S1, the lake watershed was defined using the user-friendly WWF hydroBASINS tool provided by the USGS (www.hydrosheds.org) and manually checked (Liu et al., 2020).

3.5 Statistical methods

Linear and curve fittings were conducted to determine the relationships among different variables in a PASW Statistics software (v18.0, *SPSS Inc.*). The coefficient of determination (R^2, 0 – 1) was used to measure how well a fitting model predicted the dependent variable. Pearson's r (-1 – 1) indicated the linear dependence between two variables, with $|r| > 0.7$ being highly related through a firm linear rule and $0.7 > |r| > 0.3$ being moderately correlated via a fuzzy-firm linear rule (Ratner, 2009). Moreover, we did the independent-sample t-test to check the difference between two clusters, and the results with a significance level of $p < 0.05$ (two-tailed test) were significant (Liu et al., 2023). In addition, the modelled results were evaluated using the indicators of mean absolute error (MAE), mean relative error (MRE), mean absolute percent difference (MAPD), root mean square error (RMSE), and/or bias (Eq. (4)).

$$\begin{aligned}
\text{MAE} &= (\sum\left|(POC_i^{\text{mod}} - POC_i^{\text{field}}) / POC_i^{\text{field}}\right| \cdot 100) / N \\
\text{MRE} &= (\sum((POC_i^{\text{mod}} - POC_i^{\text{field}}) / POC_i^{\text{field}}) \cdot 100)/\text{N} \\
\text{MAPD} &= (\sum\left|(POC_i^{\text{mod}} - POC_i^{\text{field}}) / POC_i^{\text{field}}\right|) \cdot 100 / N \\
\text{RMSE} &= \sqrt{\sum(POC_i^{\text{mod}} - POC_i^{\text{field}})^2 / N} \\
\text{bias} &= (\sum(POC_i^{\text{mod}} - POC_i^{\text{field}}) / (\sum POC_i^{\text{field}})) \cdot 100
\end{aligned} \tag{4}$$

where POC_i^{mod} and POC_i^{field} are the modelled and field POC concentrations for sample *i*, respectively; *N* indicates the sample size (Liu et al., 2020).

4 Algorithm development and application

4.1 Developing a blended POC algorithm

To synchronously remotely monitor lake POC in the EPL zone, previous studies indicated that water classification was priorly needed and the classification strategy depended on the bio-optical properties of POC (Jiang et al., 2019; Lin et al., 2018; Xu et al., 2021). For different lake zones in China, we also found noticeable changes in the water reflectance spectra and POC concentrations (Supplementary Fig. S1). In general, compared with western lakes in the IMXL and TPL zones, eastern lakes in the YGPL, NPML, and EPL zones had higher POC concentrations and water reflectance peak heights around 560 nm (PH_1); moreover, eastern lakes presented higher phytoplankton fluorescence peak heights around 700 nm (PH_2) for those with higher POC concentrations (Fig. S1a). In these cases, we developed a novel blended algorithm by first classifying waters into two types (I and II) using PH_1 and then calculating POC from PH_2. Three main steps were included:

[1] We calculated the equivalent remote sensing reflectance (R_{rs}) of each OLCI/Sentinel-3 band from the *in-situ* R_{field} spectra (Section 3.1) using Eq. (5):

$$R_{rs} = \int_{380}^{800} f(\lambda) R_{field}(\lambda) L(\lambda) d\lambda \Big/ \int_{380}^{800} f(\lambda) L(\lambda) d\lambda \quad (5)$$

where $f(\lambda)$ denotes the spectral response function (SRF, Fig. S1b); $L(\lambda)$ indicates the solar irradiance at the mean Earth-Sun distance (Thuillier et al., 2003).

[2] Furthermore, we calculated PH_1 using R_{rs} and selected 10% of the *in-situ* data with the lowest (Type-I) and highest (Type-II) PH_1 values to determine the independent variables for estimating POC concentrations (Figs. 2a-b). By referring to previous studies (Jiang et al., 2019; Stramska, 2005; Stramski et al., 1999), we found that a three-band *Index* and the PH_2 could be alternative indicators to predict POC in Type-I and Type-II waters, respectively (Figs. 2a-b).

[3] Finally, we tested all possible PH_1 values for dividing Type-I and Type-II waters and obtained the optimal PH_1 threshold (0.0125 sr^{-1}) with the minimum MAPD for all POC estimations. Then, *in-situ* data were used to calibrate the novel blended POC algorithm (Figs. 2c-d) shown as Eq. (6):

$$\begin{aligned}
&PH_1 = R_{rs}(560) - (R_{rs}(490) + 0.27 \times (R_{rs}(754) - R_{rs}(490))) \\
&\text{Type-I waters } (PH_1 \le 0.0125): \\
&\ln(POC) = 7.38 \times Index - 0.35 \\
&Index = R_{rs}(754)(R_{rs}(490)^{-1} - /R_{rs}(560)^{-1}) \\
&\text{Type-II waters } (PH_1 > 0.0125): \\
&\ln(POC) = -3760.87 \times [PH_2]^2 + 198.99 \times [PH_2] + 0.26 \\
&PH_2 = R_{rs}(708) - (R_{rs}(681) + 0.37 \times (R_{rs}(754) - R_{rs}(681)))
\end{aligned} \quad (6)$$

Where ln(POC) is the natural logarithm of POC; $R_{rs}(490)$, $R_{rs}(560)$, $R_{rs}(681)$, $R_{rs}(708)$, and $R_{rs}(754)$ denote the R_{rs} at the OLCI/Sentinel-3 bands with central wavelengths of 490, 560, 681, 708, and 754 nm, respectively (Figs. 2a-b).

4.2 Comparing with the published POC algorithms

Some remote sensing algorithms have been published to retrieve POC concentrations in inland and/or coastal Case-II waters (Brewin et al., 2023; Jiang et al., 2019; Liu et al., 2023). Based on the *in-situ* R_{rs} (Section 4.1), we recalibrated the published state-of-the-art POC algorithms (Jiang et al., 2019; Le et al., 2018; Liu et al., 2023; Son et al., 2009; Stramski et al., 2008). Moreover, when calibrating the band ratio algorithms, different band ratios were selected for Type-I and Type-II waters. Except for the algorithm developed by this study, the three with the smallest MADP values were the band ratio, the normalized difference carbon index (NDCI), and the color index (CI) algorithms (Table 2). Then, we compared the results modelled by the novel developed algorithm with the results of the published algorithms.

4.3 Applying the novel algorithm to OLCI/Sentinel-3 imagery

Using the novel blended POC algorithm (Eq. (6)), this study derived daily POC concentrations in 450 large lakes across China (Section 2) from the corrected OLCI/Sentinel-3 reflectance (Section 3.3). For a specific lake, land and cloud cover areas were identified by the IdePix module in the SNAP platform (Jiang et al., 2021; Liu et al., 2021); moreover, by moving a 3 × 3 window, data within two pixels near land and cloud were also excluded to weaken their adjacency effects (Feng and Hu, 2016). Finally, based on the daily results, the pixel- and lake-based monthly mean POC concentrations in July 2017 were calculated via the arithmetic average method.

5 Results

5.1 Bio-optical characteristics of Chinese lakes

Across China, lakes covered wide ranges of Chl-a (0.002 – 1131.96 μg/L), SDD (7 –1400 cm), and POC (0.13 – 41.34 mg/L) (Table 1). Overall, lake POC was sourced from both phytoplankton production and sediment resuspension. *In-situ* ln(POC) was strongly related to ln(Chl-a) (r = 0.85, p < 0.01, Fig. 3a) and moderately negatively correlated with ln(SDD) (r = -0.62, p < 0.01, Fig. 3b). However, the linear fitting coefficients of slopes and intercepts changed for different water types (Section 4.1). Moreover, for Type-II (vs. Type-I) waters with high Chl-a (43.14 ± 82.57 vs. 24.91 ± 46.55 ug/L), low SDD (31.04 ± 17.59 vs. 156.55 ± 197.8 cm), and high POC (4.65 ± 4.11 vs. 2.66 ± 3.37 mg/L), there was only a weak linear relationship between ln(POC) and ln(SDD), with r = 0.02. Namely, compared to Type-I waters, sediment resuspension contributed more to POC for Type-II waters.

The differences in POC sources differentiated the optical properties of Type-I and Type-II waters. Water reflectance for Type-I waters was high at the blue-green bands around 490 nm but low at the red-NIR bands around 708 nm (Figs. S1b, 2b). In contrast, water reflectance for Type-II waters showed evident phytoplankton absorption valleys around 681 nm and fluorescence peaks around 708 nm. Of all band ratios for OLCI/Sentinel-3 data, the best indicators for predicting POC in Type-I and Type-II waters were the $R_{rs}(708)/R_{rs}(490)$ and $R_{rs}(681)/R_{rs}(708)$ (Figs. 3c-d), which were used in the band ratio algorithm in this study (Table 2).

5.2 Performance of the developed POC algorithm

5.2.1 When applying to in-situ R_{field}

The novel blended POC algorithm outperformed the previously published algorithms (Section 4.2). For the 1269 stations with R_{field} and POC match-ups, the novel algorithm obtained satisfactory POC evaluation results of MAPD = 35.93% and RMSE = 2.64 mg/L (Fig. 4a). In comparison, for the band ratio, NDCI, and CI indicators, the MAPD values were 40.56%, 66.92%, and 76.42%, respectively; the RMSE values were 2.73 mg/L, 3.71 mg/L, and 3.71 mg/L, respectively (Table 2, Fig. 4). However, all the four algorithms overestimated POC concentrations for Type-I waters but underestimated POC for Type-II waters, especially the NDCI and CI indexes which estimated POC without prior water classification. Therefore, we believe that prior water classification could improve the estimation of POC in Chinese lakes.

5.2.2 When applying to OLCI/Sentinel-3 imagery

The novel blended POC algorithm (Eq. (6)) was then applied to the water reflectance of OLCI/Sentinal-3 (Section 3.3). For the 49 sampled lakes (Table 1), the OLCI-derived lake-based mean POC in July 2017 was strongly linearly related to the *in-situ* values, with $r = 0.85$ and $p < 0.01$. Moreover, being consistent with the *in-situ* data (Section 5.1), the OLCI-derived POC had high values in Type-II waters indicated by high Chl-a and/or TSM concentrations. For the 450 studied lakes (Fig. 1), the OLCI-derived lake-based mean POC in July 2017 exponentially elevated along with increasing both Chl-a ($R^2 = 0.52$, $p < 0.01$, Fig. 5a) and TSM

concentrations (R^2 = 0.44, p < 0.01, Fig. 5b). Moreover, the same as the *in-situ* results (Table S1), the spatial variations (the standard deviations) were more pronounced for lakes in the NPML and EPL zones with higher POC levels (Figs. 5a-b). Therefore, the novel blended algorithm can be applied to OLCI/Sentinel-3 data to retrieve lake POC across China.

5.3 Spatial variations in lake POC across China

POC concentration changed greatly across China and showed a spatial pattern of "low in the west and high in the east", which agreed with the measurements (Figs. 1, 6). Across different lakes, there was a strong positive linear correlation between lake-based mean POC in July 2017 and the lake's centroid longitude, with r = 0.71 and p < 0.01 (Fig. 6b). A similar relationship was also found for the IMXL zone oriented on an east-west axis, with r = 0.61 and p < 0.01. The spatial distributions of lake POC were mainly influenced by population density and water depth (Fig. 6). Strong human activities in the east increased lake POC (r = 0.81) by promoting algal proliferation (r = 0.47), which was also witnessed by the negative relationship between elevation and POC (r = -0.69). On the contrary, water depth decreased lake POC (r = -0.33) by weakening sediment resuspension (r = -0.39).

For a specific zone, mean POC also spatially differed across different lakes, especially in the western IMXL, TPL, and YGPL zones (Figs. 7-8). For example, although most lakes (83.21%) in the TPL zone had low POC concentrations (< 3.19 mg/L), some small lakes still presented high POC (Fig. S2). This might be due to high POC contributions of sediment resuspension in shallow lakes, which was

indicated by the positive relationship between POC concentration and water depth (r = 0.43, p < 0.01). By comparison, high POC concentrations were found for almost all lakes in the eastern NPML (100%) and EPL (90.8%) zones, where POC was mainly sourced from phytoplankton production (Fig. S2, Table S1).

POC concentration also spatially varied within a specific lake, especially for the eastern POC-rich lakes (Figs. 7-8, S3-S5). Across different lakes, the standard deviations of POC logarithmically increased along with the increasing lake-based mean values, with R^2 = 0.75 and p < 0.01. For the three typical western lakes, Bositeng, Qinghai, and Selin, POC was only 0.93 ± 0.09 mg/L, 0.88 ± 0.16 mg/L, and 0.83 ± 0.13 mg/L, respectively (Fig. S5). In contrast, POC concentrations in the three typical eastern lakes, Hulun, Dongting, and Taihu, were as high as 7.42 ± 1.92 mg/L, 2.85 ± 1.40 mg/L, and 2.27 ± 0.98 mg/L, respectively. In addition, POC generally had high values in the lake bays and/or nearshore waters, as shown in the lakes Qinghai and Taihu (Fig. S5).

6 Discussion

6.1 Strengths and limitations of the novel algorithm

Due to the absorbing aerosol types and glint/adjacency effects, accurate atmospheric correction over lakes is difficult (Kutser et al., 2016; Pahlevan et al., 2021). To weaken the effects of atmospheric correction errors, therefore, some studies directly adopted the Rayleigh-corrected reflectance to monitor lakes (Hu et al., 2010; IOCCG, 2018). Moreover, because reflectance errors tend to be spectrally flat and related (Mitchell et al., 2017), algorithms using band reflectance ratio or

difference indicators allow removing the effects to a certain extent (Hu et al., 2010; IOCCG, 2018; Kutser et al., 2016). In this study, the novel POC algorithm based on band ratio and difference is also resistant to atmospheric correction errors, especially for Type-I waters. When with ±50% errors in the *in-situ* water reflectance in Section 3.1 (Brockmann et al., 2016; Doerffer, 2010), MAR and MRE were 41.8 – 46.56% (29.91 – 58.79%) and 18.46 – 25.23% (-8.77 – 47.71%) for the Type-I (Type-II) waters, respectively (Fig. 9).

The novel POC algorithm could also obtain satisfactory results for waters covered by river plumes, minor algal blooms, and/or thin clouds. For the turbid estuaries (Lakes Bositeng and Dongting), lake bays (Lakes Qinghai and Selin), and waters near algal blooms (Lake Taihu), the expected high POC concentrations were retrieved (Fig. 10). Moreover, the OLCI-derived POC in thin cloud-covered waters (Lake Hulun) did not show abnormally high/low values. In addition, the novel POC algorithm could be extended to other ocean color satellite sensors, equipping bands for the water reflectance peak around 560 nm and phytoplankton fluorescence peak around 700 nm, for example the MODerate-resolution Imaging Spectroradiometer (Brockmann et al., 2016; Huang et al., 2019).

The novel algorithm might have limitations in two aspects. Firstly, it might achieve a higher accuracy by classifying waters into more types. Based on the reflectance spectrum shapes, Spyrakos et al. (2018) resolved 13 spectrally distinct lake types globally. Further studies may build on this work by investigating the sensitivities of the algorithm to an increasing number of bio-optical water types.

Secondly, it might be insensitive to sediment-sourced POC for Type-II waters. The novel algorithm adopted the phytoplankton fluorescence peak height near 708 nm (PH_2) (Gower et al., 1999; IOCCG, 2018) to calculate POC in Type-II waters (Eq. (6)). Nevertheless, PH_2 is not sensitive to sediment-related POC, because the absorption and backscattering spectra of suspended sediment exponentially decrease to low values and are spectrally flat around 708 nm (Cael and Boss, 2017; Sun et al., 2010). This might be one reason for the underestimation of POC concentrations in some turbid estuaries, such as Lakes Bositeng and Selin (Figs. 10, S5).

6.2 Impacts factors on POC retrieval

6.2.1 The POC:Chl-a ratio

POC:Chl-a ratio is an essential factor impacting POC retrieval. For waters where POC is mainly sourced from phytoplankton, the satellite-derived Chl-a is commonly adopted to estimate POC (Jiang et al., 2015; Stramska, 2005; Stramski et al., 1999, 2008). The novel algorithm also estimated POC from Chl-a fluorescence peak height for Type-II waters (Section 4.1). However, POC:Chl-a (or carbon:Chl-a) spatiotemporally varies under different biogeochemistry conditions (Geider, 1987; Jakobsen and Markager, 2016; Sathyendranath et al., 2009). For the sampled lakes, POC:Chl-a ranged from 0.07 to 10.52 mg/ug and presented an apparent spatial pattern of "high in the west and low in the east" (Fig. 11a). Moreover, compared to Type-I waters, Type-II waters had significantly higher Chl-a concentrations but lower POC:Chl-a ratios ($p < 0.05$, *t*-test, Figs. 11b-c).

There are three possible explanations for the spatial pattern of POC:Chl-a ratio. ① Eutrophication increased Chl-a (Hou et al., 2022; Liu et al., 2023) but decreased POC:Chl-a ratios in the eastern lakes (R^2 = 0.57, p < 0.01). ② Along with a chlorosis adaption of phytoplankton (Geider, 1987; Wang et al., 2008), low air temperature elevated POC:Chl-a ratios in the western lakes (R^2 = 0.36, p < 0.01, Fig. 11d). ③ Diatom dominance (Sathyendranath et al., 2009) and nitrogen reduction (Jakobsen and Markager, 2016) could elevate carbon:Chl-a, which also contributed to the high POC:Chl-a ratios in the western oligotrophic lakes (NIGLAS, 2019). In these cases, the relationship between POC and Chl-a varied across water types (Fig. 11e), which further influenced the POC calculation based on Chl-a.

6.2.2 Suspended sediment composition

Because suspended sediment dominates POC sources in some waters (Jiang et al., 2019; Lin et al., 2018), Chl-a was only moderately related to POC for all the *in-situ* match-ups (N = 1234; r = 0.61). The suspended sediment composition also affects POC inversion accuracy. First, suspended sediment contributes significantly to the reflectance of shallow turbid lakes, which leads to significant uncertainties in estimating Chl-a (Liu et al., 2023; Sun et al., 2010). Second, there are spatial variations in the weight percent of POC in sediment (%POC), which is linearly correlated with the loss-on-ignition for lakes in the EPL zone (Dong et al., 2012). Third, the %POC decreases with the increase in the particle size of suspended sediment (Qu et al., 2020). Therefore, more work is needed to improve POC inversion by considering suspended sediment composition.

6.3 Implications for estimating lake POC storage

Lakes act as an important POC reservoir (Liu et al., 2023; Tranvik et al., 2009). Moreover, water column-integrated POC storage is related to carbon cycle processes such as photosynthesis, flocculation, and oxidative decomposition (Jiao et al., 2010; Regnier et al., 2022; Tranvik et al., 2009). Despite the importance, research on lake POC storage is still very limited. Chen et al. (2015) simply assumed that POC accounted for 10% of the total organic carbon when estimating lake POC storage globally, which might greatly underestimated POC storage in eutrophic and/or shallow lakes. For the eutrophic Lake Taihu in China, POC accounted for 23.39% – 68.72% of the total organic carbon content (Song et al., 2008). Because of its importance and spatiotemporal variations, remote monitoring of POC storage is necessary for better understanding the lake carbon cycle.

Based on the OLCI-derived surface POC concentration (Section 5.3), lake POC storage could be further estimated via three strategies: ① classification method assuming a fixed POC profile for each water type (Cui, 2017); ② empirical method using the relationship between POC storage and concentration (Duforêt-Gaurier et al., 2010); ③ process-oriented method by remotely parameterizing POC profiles (Liu et al., 2023). However, lake POC profiles vary spatiotemporally; for the Type-I Lake Fuxian, POC profiles presented as vertically mixed decay or Gauss peak types (Figs. 12a-b); for the Type-II Lake Chaohu, however, POC profiles showed uniform, exponential decay, or power decay types (Figs. 12c-d). In these cases, the relationship between surface POC concentration

and POC storage was strong for Lake Fuxian (r = 0.85) but only moderately for Lake Chaohu (r = 0.53). Therefore, like oceans (Cui, 2017; Duforêt-Gaurier et al., 2010), POC storage in Type-I lakes could simply use the empirical or classification method; however, the process-oriented method is recommended for Type-II lakes (Liu et al., 2023).

7 Conclusions

Based on the bio-optical properties in 49 lakes across China (N = 1269), this study developed a novel blended POC inversion algorithm, which obtained a lower MAPD (35.93%) than three previously published formulas (40.56% – 76.42%) and could be applied to OLCI/Sentinel-3 imagery. However, the POC:Chl-a ratio and suspended sediment composition should be considered so as to improve POC estimation. The OLCI-derived lake POC concentration in China showed an obvious spatial pattern of "low in the west and high in the east". Furthermore, the OLCI-derived POC concentration could be used to estimate POC storage in Type-I lakes by an empirical or classification way, but a process-oriented method is required for Type-II lakes. This study is significant for dynamically monitoring the lake carbon cycle on a large spatial scale using satellite data.

Acknowledgments

We thank the European Space Agency for providing the OLCI/Sentinel-3 satellite data and all Lake Environment Remote Sensing Group members for their help in the field investigation. This study was supported by the Natural Science Foundation of Jiangsu Province (Grants #BK20220018 and #BK20181102), the

National Natural Science Foundation of China (Grants #42271376, #U2243205, and #41901299), the Youth Innovation Promotion Association CAS (Grant #2021313), and the NIGLAS Foundation (Grant #E1SL002).

References

Artifon, V., Zanardi-Lamardo, E., & Fillmann, G. (2019). Aquatic organic matter: Classification and interaction with organic microcontaminants. *Science of the Total Environment, 649*, 1620-1635.

Bastviken, D., Tranvik, L.J., Downing, J.A., Crill, P.M., & Enrich-Prast, A. (2011). Freshwater methane emissions offset the continental carbon sink. *Science, 331*, 50.

Brewin, R.J.W., Sathyendranath, S., Kulk, G., Rio, M.-H., Concha, J.A., Bell, T.G., Bracher, A., Fichot, C., Frölicher, T.L., Galí, M., Hansell, D.A., Kostadinov, T.S., Mitchell, C., Neeley, A.R., Organelli, E., Richardson, K., Rousseaux, C., Shen, F., Stramski, D., Tzortziou, M., Watson, A.J., Addey, C.I., Bellacicco, M., Bouman, H., Carroll, D., Cetinić, I., Dall'Olmo, G., Frouin, R., Hauck, J., Hieronymi, M., Hu, C., Ibello, V., Jönsson, B., Kong, C.E., Kovač, Ž., Laine, M., Lauderdale, J., Lavender, S., Livanou, E., Llort, J., Lorinczi, L., Nowicki, M., Pradisty, N.A., Psarra, S., Raitsos, D.E., Ruescas, A.B., Russell, J.L., Salisbury, J., Sanders, R., Shutler, J.D., Sun, X., Taboada, F.G., Tilstone, G.H., Wei, X., & Woolf, D.K. (2023). Ocean carbon from space: Current status and priorities for the next decade. *Earth-Science Reviews, 240*, 104386.

Brockmann, C., Doerffer, R., Peters, M., Stelzer, K., Embacher, S., & Ruescas, A. (2016). Evolution of the C2RCC neural network from Sentinel 2 and 3 for the retrieval of ocean colour products in normal and extreme optically complex waters. *ESASP, 740*.

Cael, B.B., & Boss, E. (2017). Simplified model of spectral absorption by non-algal particles and dissolved organic materials in aquatic environments. *Optics Express, 25*, 25486-25491.

Chen, M., Zeng, G., Zhang, J., Xu, P., Chen, A., & Lu, L. (2015). Global landscape of total organic carbon, nitrogen and phosphorus in Lake Water. *Scientific Reports, 5*, 15043.

Cui, W. (2017). Remote sensing estimation of organic carbon storage in the euoptical layer of the northern South China Sea. *Hangzou: Second Institute of Oceanography, Ministry of Natural Resources*.

Doerffer, R. (2010). OLCI level 2 algorithm theoretical basis document: Ocean colour turbid water.

Dong, X., Anderson, N.J., Yang, X., chen, X., & Shen, J. (2012). Carbon burial by shallow lakes on the Yangtze floodplain and its relevance to regional carbon sequestration. *Global Change Biology, 18*, 2205-2217.

Drake, T.W., Raymond, P.A., & Spencer, R.G.M. (2017). Terrestrial carbon inputs to inland waters: A current synthesis of estimates and uncertainty. *Limnology and Oceanography Letters, 3*, 132-142.

Duforêt-Gaurier, L., Loisel, H., Dessailly, D., Nordkvist, K., & Alvain, S. (2010). Estimates of particulate organic carbon over the euphotic depth from in situ measurements. Application to satellite data over the global ocean. *Deep Sea Research Part I: Oceanographic Research Papers, 57*, 351-367.

Feng, L., & Hu, C. (2016). Cloud adjacency effects on top-of-atmosphere radiance and ocean color data products: A statistical assessment. *Remote Sensing of Environment, 174*, 301-313.

Geider, R.J. (1987). Light and temperature dependence of the carbon to chlorophyll a ratio in microalgae and cyanobacteria: Implication for physiology and growth of phytoplankton. *New Phytologist, 106*, 1-34.

Gower, J.F.R., Doerffer, R., & Borstad, G.A. (1999). Interpretation of the 685 nm peak in water-leaving radiance spectra in terms of fluorescence, absorption and scattering, and its observation by MERIS. *International Journal of Remote Sensing, 20*, 1771-1786..

Hou, X., Feng, L., Dai, Y., Hu, C., Gibson, L., Tang, J., Lee, Z., Wang, Y., Cai, X., Liu, J., Zheng, Y., & Zheng, C. (2022). Global mapping reveals increase in lacustrine algal blooms over the past decade. *Nature Geoscience, 15*, 130-134

Hu, C., Lee, Z., Ma, R., Yu, K., Li, D., & Shang, S. (2010). Moderate Resolution Imaging Spectroradiometer (MODIS) observations of cyanobacteria blooms in Taihu Lake, China. *Journal of Geophysical Research, 115*.

Huang, C., Zhang, Y., Huang, T., Yang, H., Li, Y., Zhang, Z., He, M., Hu, Z., Song, T., & Zhu, A.X. (2019). Long-term variation of phytoplankton biomass and physiology in Taihu lake as observed via MODIS satellite. *Water Research, 153*, 187-199.

IOCCG (2018). Earth Observations in Support of Global Water Quality Monitoring. Greb, S., Dekker, A. and Binding, C. (eds.), IOCCG Report Series, No. 17, International Ocean Colour Coordinating Group, Dartmouth, Canada.

Jakobsen, H.H., & Markager, S. (2016). Carbon-to-chlorophyll ratio for phytoplankton in temperate coastal waters: Seasonal patterns and relationship to nutrients. *Limnology and Oceanography, 61*, 1853-1868.

Jiang, D., Matsushita, B., Pahlevan, N., Gurlin, D., Lehmann, M.K., Fichot, C.G., Schalles, J., Loisel, H., Binding, C., Zhang, Y., Alikas, K., Kangro, K., Uusõue, M., Ondrusek, M., Greb, S., Moses, W.J., Lohrenz, S., & O'Donnell, D. (2021). Remotely estimating total suspended solids concentration in clear to extremely turbid waters using a novel semi-analytical method. *Remote Sensing of Environment, 258*, 112386.

Jiang, G., Loiselle, S.A., Yang, D., Gao, C., Ma, R., Su, W., & Duan, H. (2019). An absorption-specific approach to examining dynamics of particulate organic carbon from VIIRS observations in inland and coastal waters. *Remote Sensing of Environment, 224*, 29-43.

Jiang, G., Ma, R., Loiselle, S.A., Duan, H., Su, W., Cai, W., Huang, C., Yang, J., & Yu, W. (2015). Remote sensing of particulate organic carbon dynamics in a eutrophic lake (Taihu Lake, China). *Science of the Total Environment, 532*, 245-254.

Jiao, N., Herndl, G.J., Hansell, D.A., Benner, R., Kattner, G., Wilhelm, S.W., Kirchman, D.L., Weinbauer, M.G., Luo, T., Chen, F., & Azam, F. (2010). Microbial production of recalcitrant dissolved organic matter: Long-term carbon storage in the global ocean. *Nature Reviews Microbiology, 8*, 593-599.

Knap, A.H., Michaels, A.F., Close, A.R., Ducklow, H.W., & Dickson, A.G. (1996). Protocols for the Joint Global Ocean Flux Study (JGOFS) core measurements. *JGOFS*.

Kutser, T., Casal Pascual, G., Barbosa, C., Paavel, B., Ferreira, R., Carvalho, L., & Toming, K. (2016). Mapping inland water carbon content with Landsat 8 data. *International Journal of Remote Sensing, 37*, 2950-2961

Le, C., Zhou, X., Hu, C., Lee, Z., Li, L., & Stramski, D. (2018). A color-index-based empirical algorithm for determining particulate organic carbon concentration in the ocean from satellite observations. *Journal of Geophysical Research: Oceans, 123*.

Lin, J., Lyu, H., Miao, S., Pan, Y., Wu, Z., Li, Y., & Wang, Q. (2018). A two-step approach to mapping particulate organic carbon (POC) in inland water using OLCI images. *Ecological Indicators, 90*, 502-512.

Liu, D., Duan, H., Loiselle, S., Hu, C., Zhang, G., Li, J., Yang, H., Thompson, J.R., Cao, Z., Shen, M., Ma, R., Zhang, M., & Han, W. (2020). Observations of water transparency in China's lakes from space. *International Journal of Applied Earth Observation and Geoinformation, 92*, 102187.

Liu, D., Sun, Z., Shen, M., Tian, L., Yu, S., Jiang, X., & Duan, H. (2023). Three-dimensional observations of particulate organic carbon in shallow eutrophic lakes from space. *Water Research, 229*, 119519.

Liu, X., Steele, C., Simis, S., Warren, M., Tyler, A., Spyrakos, E., Selmes, N., & Hunter, P. (2021). Retrieval of Chlorophyll-a concentration and associated product uncertainty in optically diverse lakes and reservoirs. *Remote Sensing of Environment, 267*, 112710.

Ma, R., Duan, H., Hu, C., Feng, X., Li, A., Ju, W., Jiang, J., & Yang, G. (2010). A half-century of changes in China's lakes: Global warming or human influence?. *Geophysical Research Letters, 37*.

Mendonca, R., Muller, R.A., Clow, D., Verpoorter, C., Raymond, P., Tranvik, L.J., & Sobek, S. (2017). Organic carbon burial in global lakes and reservoirs. *Nature Communications, 8*, 1694.

Messager, M.L., Lehner, B., Grill, G., Nedeva, I., & Schmitt, O. (2016). Estimating the volume and age of water stored in global lakes using a geo-statistical approach. *Nature Communications, 7*, 13603.

Mitchell, C., Hu, C., Bowler, B., Drapeau, D., & Balch, W.M. (2017). Estimating particulate inorganic carbon concentrations of the global ocean from ocean color measurements using a reflectance difference approach. *Journal of Geophysical Research: Oceans, 122*, 8707-8720.

Mobley, C.D. (1999). Estimation of the remote-sensing reflectance from above-surface measurements. *Applied Optics, 38*, 7442-7455.

Mueller, J.L., Fargion, G.S., & McClain, C.R. (2003). Mueller, J. L., Fargion, G. S., and McClain, C. R. (Eds.): Ocean optics protocols for satellite ocean color sensor validation, revision 4, volume III: Radiometric measurements and data analysis protocols,

NASA/TM-2003-211621/Rev4-Vol. III, NASA Goddard Space Flight Center, Greenbelt, Maryland, 78 pp., 2003.

NIGLAS (2019). Nanjing Institute of Geography and Limnology, Chinese Academy of Sciences (NIGLAS). Lake Survey Report in China. *Beijing: Science Press*.

Pahlevan, N., Mangin, A., Balasubramanian, S.V., Smith, B., Alikas, K., Arai, K., Barbosa, C., Bélanger, S., Binding, C., Bresciani, M., Giardino, C., Gurlin, D., Fan, Y., Harmel, T., Hunter, P., Ishikaza, J., Kratzer, S., Lehmann, M.K., Ligi, M., Ma, R., Martin-Lauzer, F.-R., Olmanson, L., Oppelt, N., Pan, Y., Peters, S., Reynaud, N., Sander de Carvalho, L.A., Simis, S., Spyrakos, E., Steinmetz, F., Stelzer, K., Sterckx, S., Tormos, T., Tyler, A., Vanhellemont, Q., & Warren, M. (2021). ACIX-Aqua: A global assessment of atmospheric correction methods for Landsat-8 and Sentinel-2 over lakes, rivers, and coastal waters. *Remote Sensing of Environment, 258*, 112366.

Qu, Y., Jin, Z., Wang, J., Wang, Y., Xiao, J., Gou, L.F., Zhang, F., Liu, C.Y., Gao, Y., Suarez, M.B., & Xu, X. (2020). The sources and seasonal fluxes of particulate organic carbon in the Yellow River. *Earth Surface Processes and Landforms, 45*, 2004-2019.

Ratner, B. (2009). The correlation coefficient: Its values range between +1/−1, or do they?. *Journal of Targeting, Measurement and Analysis for Marketing, 17*, 139-142.

Raymond, P.A., Hartmann, J., Lauerwald, R., Sobek, S., McDonald, C., Hoover, M., Butman, D., Striegl, R., Mayorga, E., Humborg, C., Kortelainen, P., Durr, H., Meybeck, M., Ciais, P., & Guth, P. (2013). Global carbon dioxide emissions from inland waters. *Nature, 503*, 355-359.

Regnier, P., Resplandy, L., Najjar, R.G., & Ciais, P. (2022). The land-to-ocean loops of the global carbon cycle. *Nature, 603*, 401-410.

Sathyendranath, S., Stuart, V., Nair, A., Oka, K., Nakane, T., Bouman, H., Forget, M.H., Maass, H., & Platt, T. (2009). Carbon-to-chlorophyll ratio and growth rate of phytoplankton in the sea. *Marine Ecology Progress Series, 383*, 73-84.

Son, Y.B., Gardner, W.D., Mishonov, A.V., & Richardson, M.J. (2009). Multispectral remote-sensing algorithms for particulate organic carbon (POC): The Gulf of Mexico. *Remote Sensing of Environment, 113*, 50-61.

Song, J.M., Xu, Y.F., Hu, W.P., & Ni, L.Y. (2008). Biogeochemistry of Carbon in China Seas and Lakes. *Beijing: Chinese Science Press*.

Song, K., Wang, Q., Liu, G., Jacinthe, P.A., Li, S., Tao, H., Du, Y., Wen, Z., Wang, X., Guo, W., Wang, Z., Shi, K., Du, J., Shang, Y., Lyu, L., Hou, J., Zhang, B., Cheng, S., Lyu, Y., & Fei, L. (2022). A unified model for high resolution mapping of global lake (>1 ha) clarity using Landsat imagery data. *Science of the Total Environment, 810*, 151188.

Spyrakos, E., O'Donnell, R., Hunter, P.D., Miller, C., Scott, M., Simis, S.G.H., Neil, C., Barbosa, C.C.F., Binding, C.E., Bradt, S., Bresciani, M., Dall'Olmo, G., Giardino, C., Gitelson, A.A., Kutser, T., Li, L., Matsushita, B., Martinez-Vicente, V., Matthews, M.W., Ogashawara, I., Ruiz-Verdú, A., Schalles, J.F., Tebbs, E., Zhang, Y., & Tyler, A.N. (2018). Optical types of inland and coastal waters. *Limnology and Oceanography, 63*, 846-870.

Stramska, M. (2005). Variability of particulate organic carbon concentration in the north polar Atlantic based on ocean color observations with Sea-viewing Wide Field-of-view Sensor (SeaWiFS). *Journal of Geophysical Research, 110*.

Stramski, D., Joshi, I., & Reynolds, R.A. (2022). Ocean color algorithms to estimate the concentration of particulate organic carbon in surface waters of the global ocean in support of a long-term data record from multiple satellite missions. *Remote Sensing of Environment, 269*, 112776.

Stramski, D., Reynolds, R.A., Babin, M., Kaczmarek, Lewis, M.R., Röttgers, R., Sciandra, A., Stramska, M., Twardowski, M.S., Franz, B.A., & Claustre, a.H. (2008). Relationships between the surface concentration of particulate organic carbon and optical properties in the eastern South Pacific and eastern Atlantic Oceans. *Biogeosciences, 5*, 171-201.

Stramski, D., Reynolds, R.A., Kahru, M., & Mitchell, B.G. (1999). Estimation of particulate organic carbon in the ocean from satellite remote sensing. *Science, 285*, 239-242.

Sun, D., Li, Y., Wang, Q., Lv, H., Le, C., Huang, C., & Gong, S. (2010). Partitioning particulate scattering and absorption into contributions of phytoplankton and non-algal particles in winter in Lake Taihu (China). *Hydrobiologia, 644*, 337-349.

Thuillier, G., HersÉ, M., Labs, D., Foujols, T., Peetermans, W., Gillotay, D., Simon, P.C., & Mandel, H. (2003). The Solar Spectral Irradiance from 200 to 2400 nm as Measured by the SOLSPEC Spectrometer from the Atlas and Eureca Missions. *Solar Physics, 214*, 1-22.

Tranvik, L.J., Downing, J.A., Cotner, J.B., Loiselle, S.A., Striegl, R.G., Ballatore, T.J., Dillon, P., Finlay, K., Fortino, K., Knoll, L.B., Kortelainen, P.L., Kutser, T., Larsen, S., Laurion, I., Leech, D.M., McCallister, S.L., McKnight, D.M., Melack, J.M., Overholt, E., Porter, J.A., Prairie, Y., Renwick, W.H., Roland, F., Sherman, B.S., Schindler, D.W., Sobek, S., Tremblay, A., Vanni, M.J., Verschoor, A.M., Wachenfeldt, E.v., & Weyhenmeyer, G.A. (2009). Lakes and reservoirs as regulators of carbon cycling and climate. *Limnology and Oceanography, 54*, 2298-2314.

Wang, S., Gao, Y., Jia, J., Lu, Y., Sun, K., Ha, X., Li, Z., & Deng, W. (2021). Vertically stratified water source characteristics and associated driving mechanisms of particulate organic carbon in a large floodplain lake system. *Water Research, 209*, 117963.

Wang, X.J., Behrenfeld, M., Borgne, R.L., Murtugudde, R., & Boss, E. (2008). Regulation of phytoplankton carbon to chlorophyll ratio by light, nutrients and temperature in the equatorial Pacific Ocean: A basin-scale model. *Biogeosciences Discussions, 5*, 3869-3903.

Xu, J., Li, Y., Lyu, H., Lei, S., Mu, M., Bi, S., Xu, J., Xu, X., Miao, S., Li, L., & Yan, X. (2021). Simultaneous inversion of concentrations of POC and its endmembers in lakes: A novel remote sensing strategy. *Science of the Total Environment, 770*, 145249.

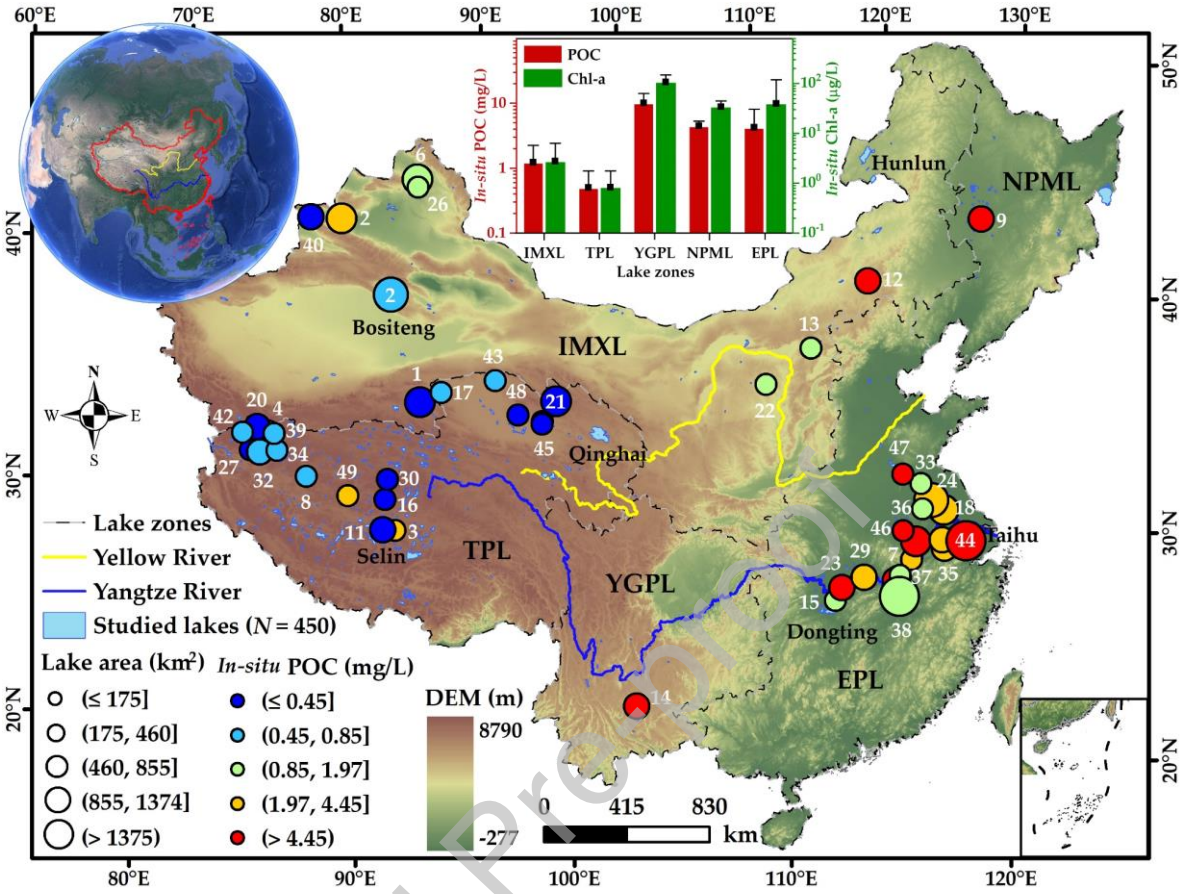

Fig. 1. All studied lakes and the sampled lakes in China. Lake code and mean *in-situ* POC concentration are shown (Table 1). The digital elevation model (DEM) acquired via the Shuttle Radar Topography Mission (SRTM) was sourced from the National Aeronautics and Space Administration (NASA) (www.earthdata.nasa.gov). The white numbers indicate lake codes shown in Table 1. The aerial view in the top left corner was obtained from Google Earth.

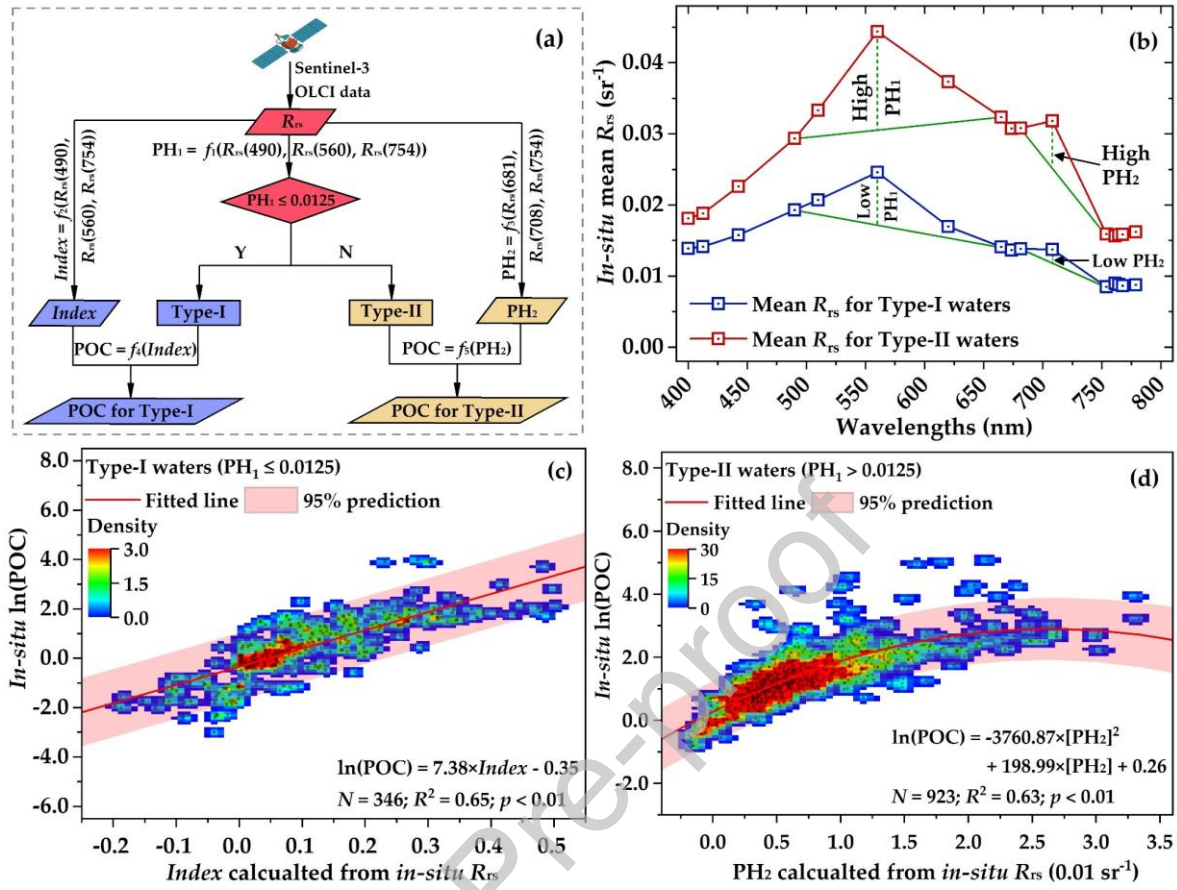

Fig. 2. Algorithm development and calibration. (a) Binary decision tree for developing the blended algorithm. (b) Equivalent R_{rs} at the OLCI/Sentinel-3 bands for two types of waters. (c – d) POC estimation equations for Type-I and Type-II waters, respectively.

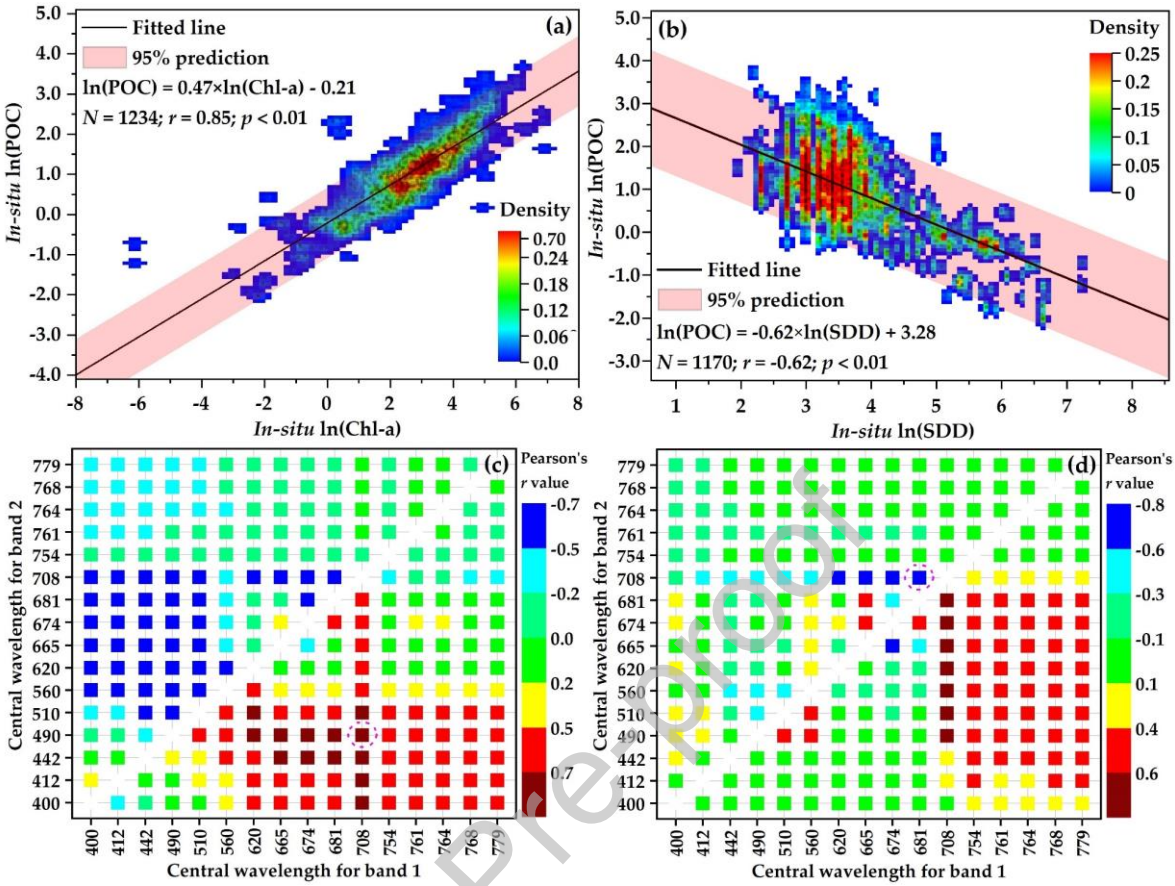

Fig. 3. The bio-optical properties of lake POC. The linear correlations (a) between ln(POC) and ln(Chl-a) and (d) between ln(POC) and ln(SDD). The *r* values of the linear relationships between band ratio (band1/band2) and ln(POC) for (a) Type-I and (b) Type-II waters. The red dotted circles denote the ratios which get the highest *r* values.

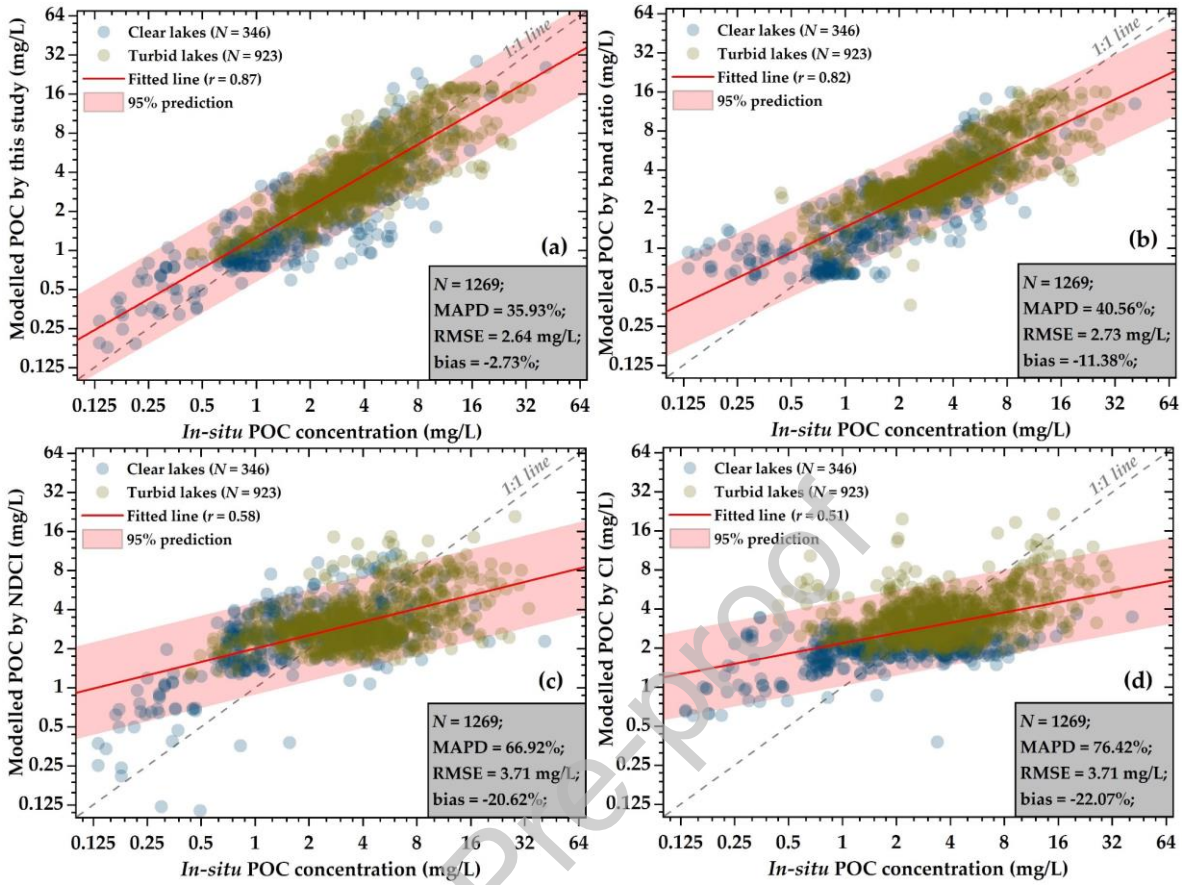

Fig. 4. Validation for POC concentrations modelled using (a) the novel blended algorithm (Eq. (6)), (b) the band ratio, (c) the NDCI, and (d) the CI algorithms (Table 2).

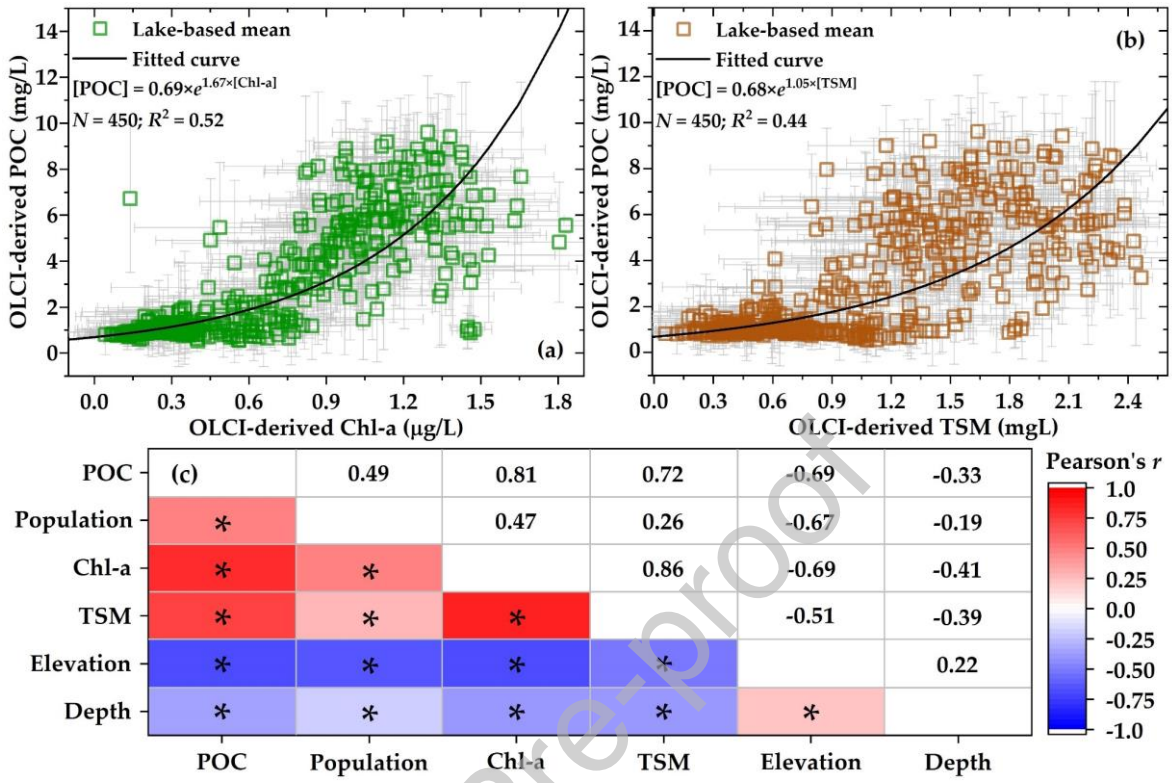

Fig. 5. Relationships between the OLCI-derived POC and (a) Chl-a, (b) TSM, and (c) other environmental factors. Chl-a and TSM were retrieved using Eq. (3). Symbol '*' indicates the significant correlations ($p < 0.01$).

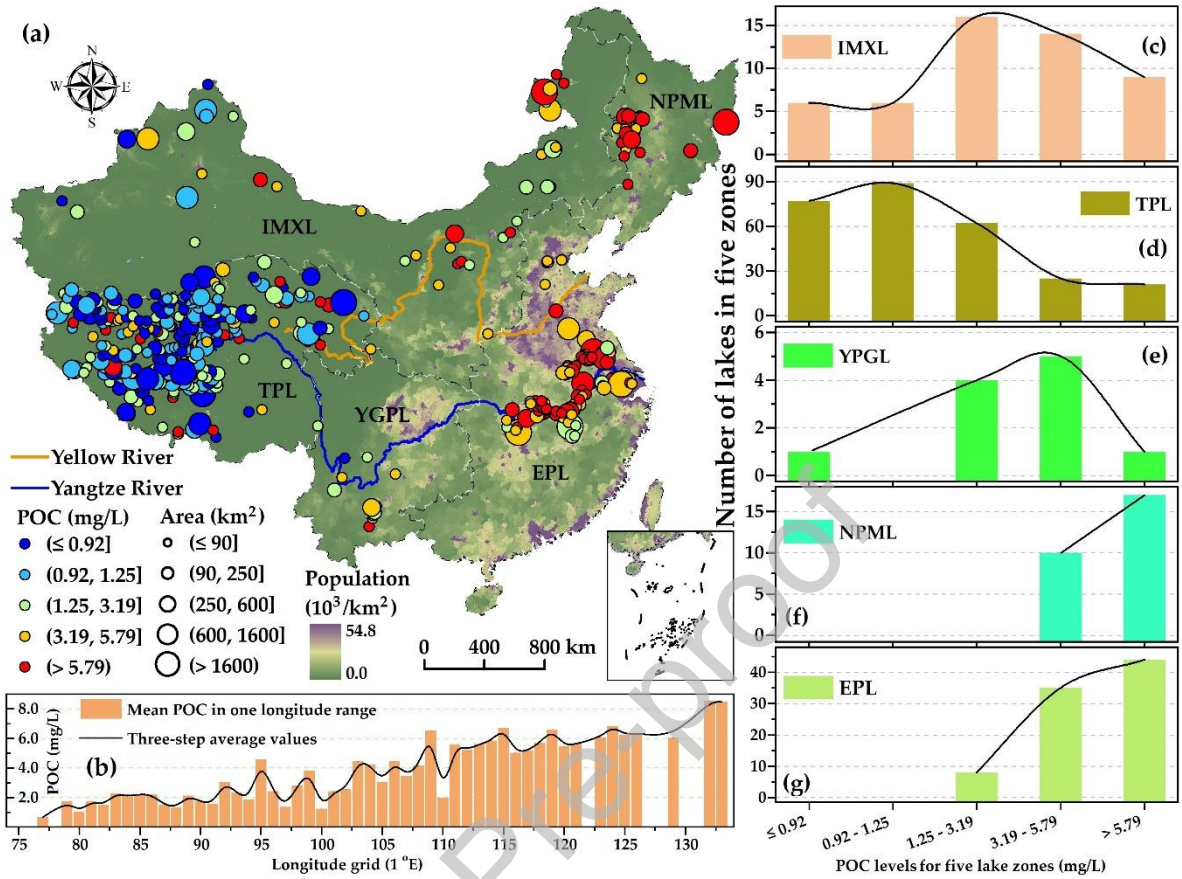

Fig. 6. The OLCI-derived mean POC concentrations in 450 large lakes. (a) The lake-based mean POC. (b) Mean POC in grid longitude from west to east. (c – g) are the histograms of POC levels for the five lake zones. OLCI/Sentinel-3 data in July 2017 were employed to derive POC.

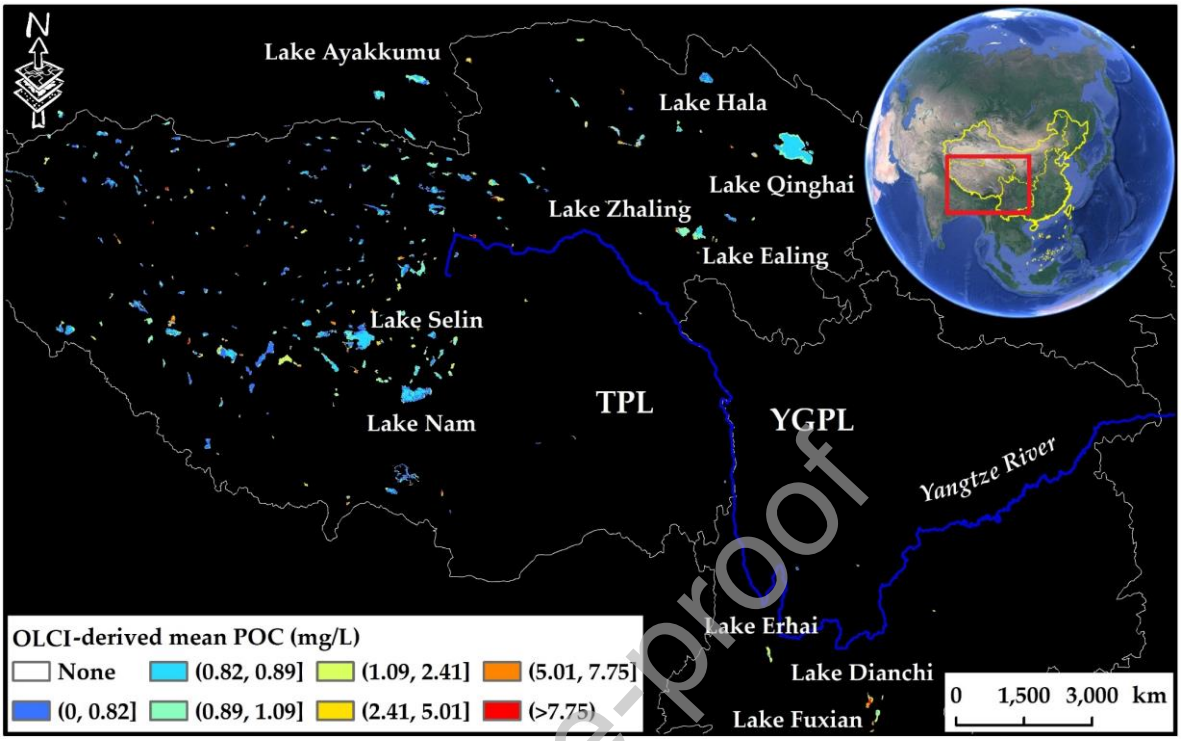

Fig. 7. OLCI-derived mean POC concentrations in lakes across the TPL and YGPL zones. The OLCI/Sentinel-3 data in July 2017 (Section 3.3) were adopted to retrieve POC. The inserted aerial view was obtained from Google Earth.

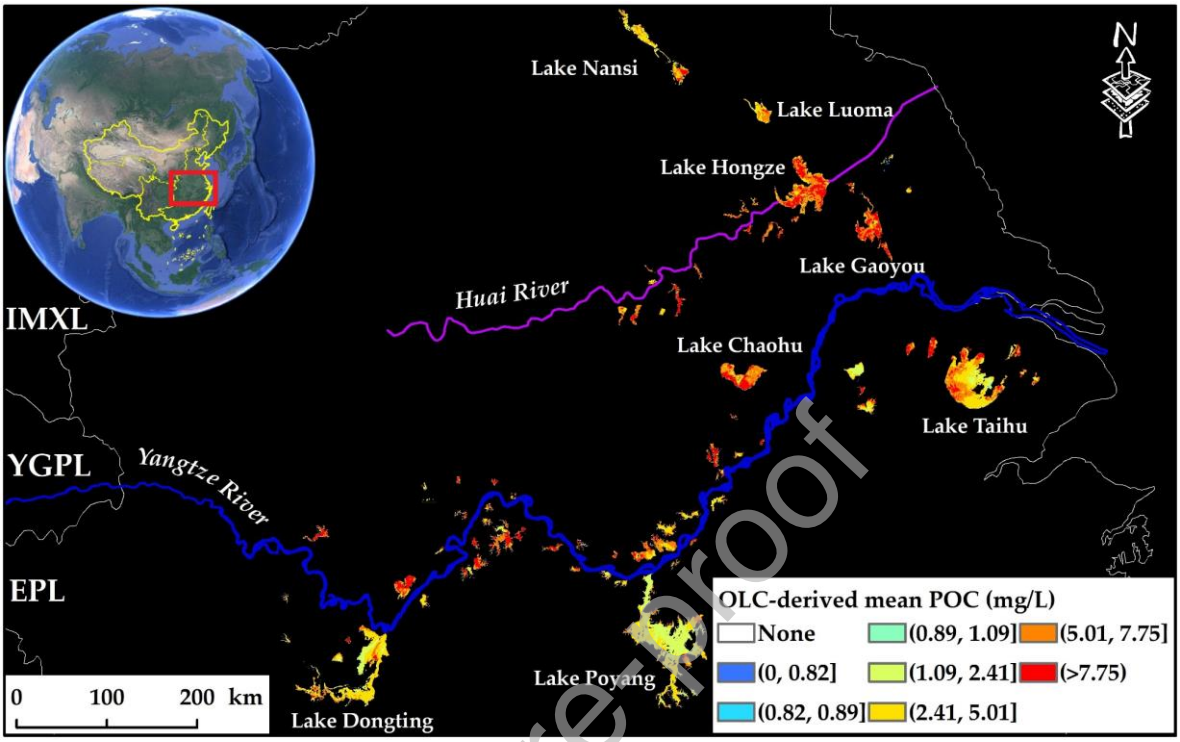

Fig. 8. OLCI-derived mean POC concentrations in lakes across the EPL zone. OLCI/Sentinel-3 data in July 2017 (Section 3.3) were adopted to derive POC. The inserted aerial view was obtained from Google Earth.

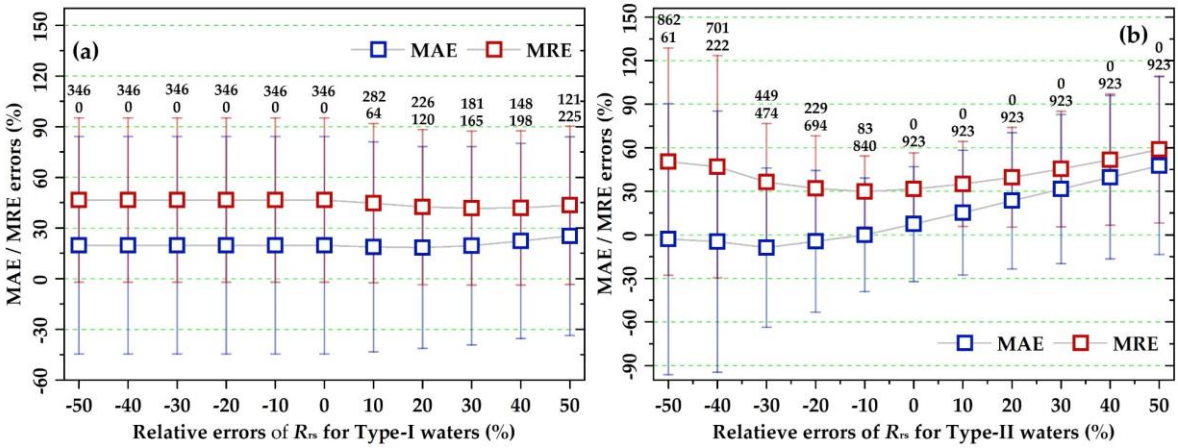

Fig. 9. Sensitivities of the novel algorithm to assumed errors in *in-situ* R_{field} for (a) Type-I and (b) Type-II waters. The numbers show how many stations were reclassified as Type-I (up) and Type-II (down) under different conditions.

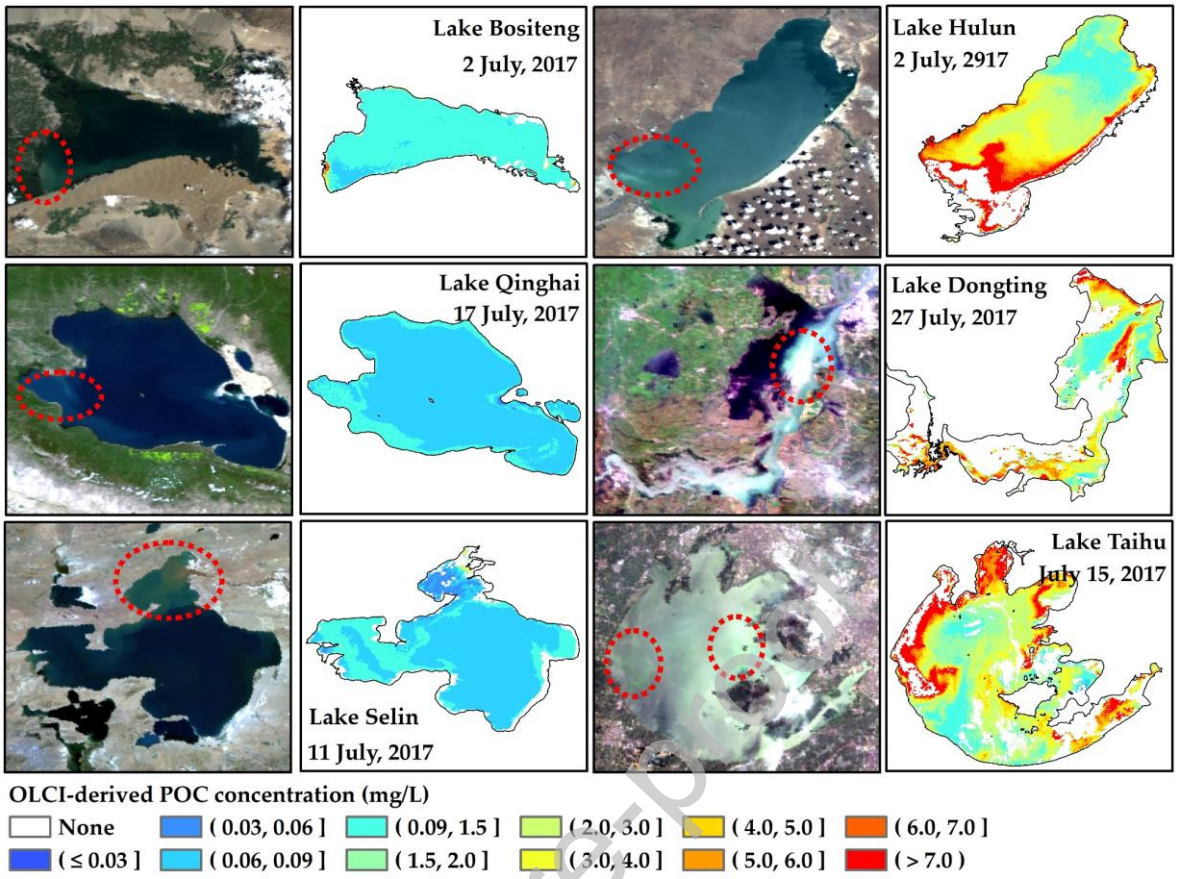

Fig. 10. OLCI-derived POC for the six typical lakes across China. The red dashed ellipses indicate the turbid estuary waters (Lakes Bositeng and Dongting), turbid bay waters (Lakes Qinghai and Selin), cloud-covered waters (Lake Hulun), or algal bloom waters (Lake Taihu).

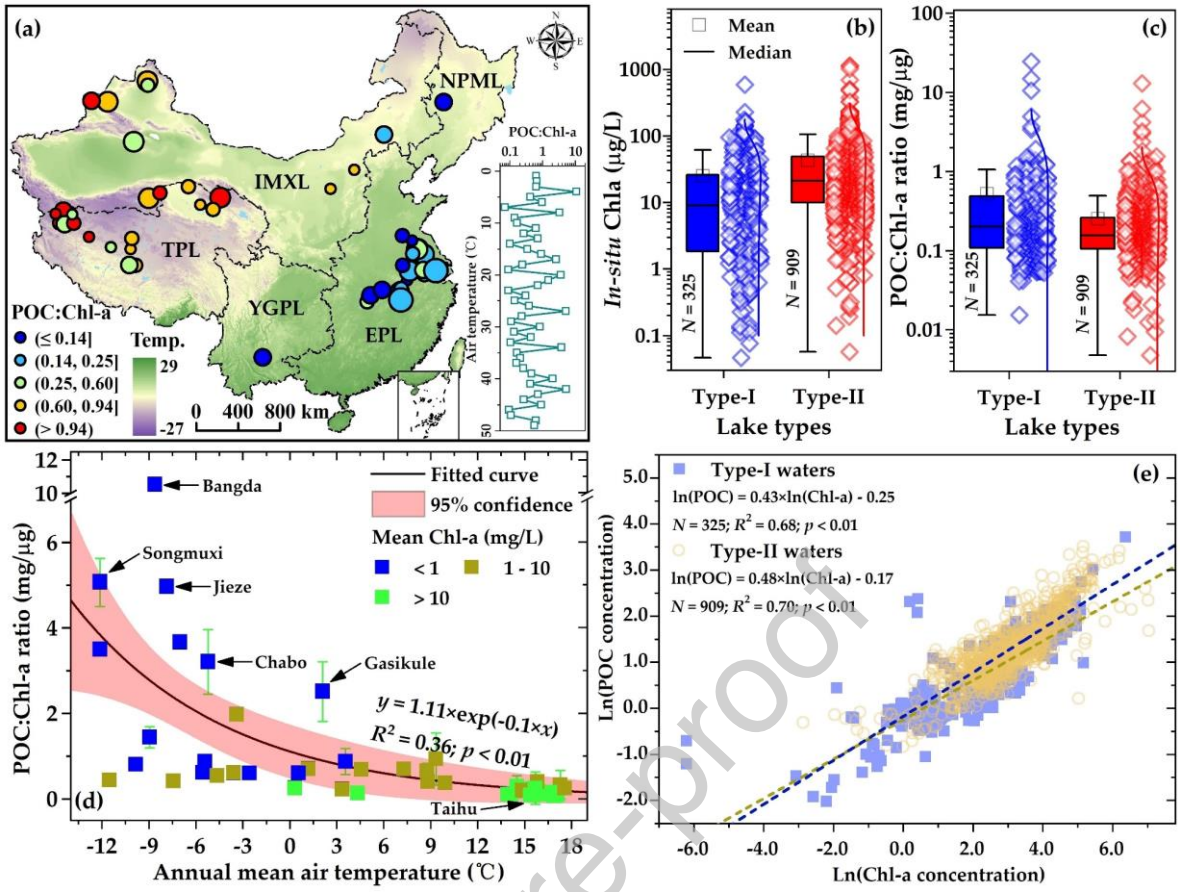

Fig. 11. Variations in the POC:Chl-a ratios. (a) Mean POC:Chl-a in the sampled lakes. (b – c) The histograms of *in-situ* Chl-a and POC:Chl-a for Type-I and Type-II waters. (d) The exponential dependence of the POC:Chl-a ratio on air temperature. (e) Linear relationships between ln(POC) and ln(Chl-a) for two water types.

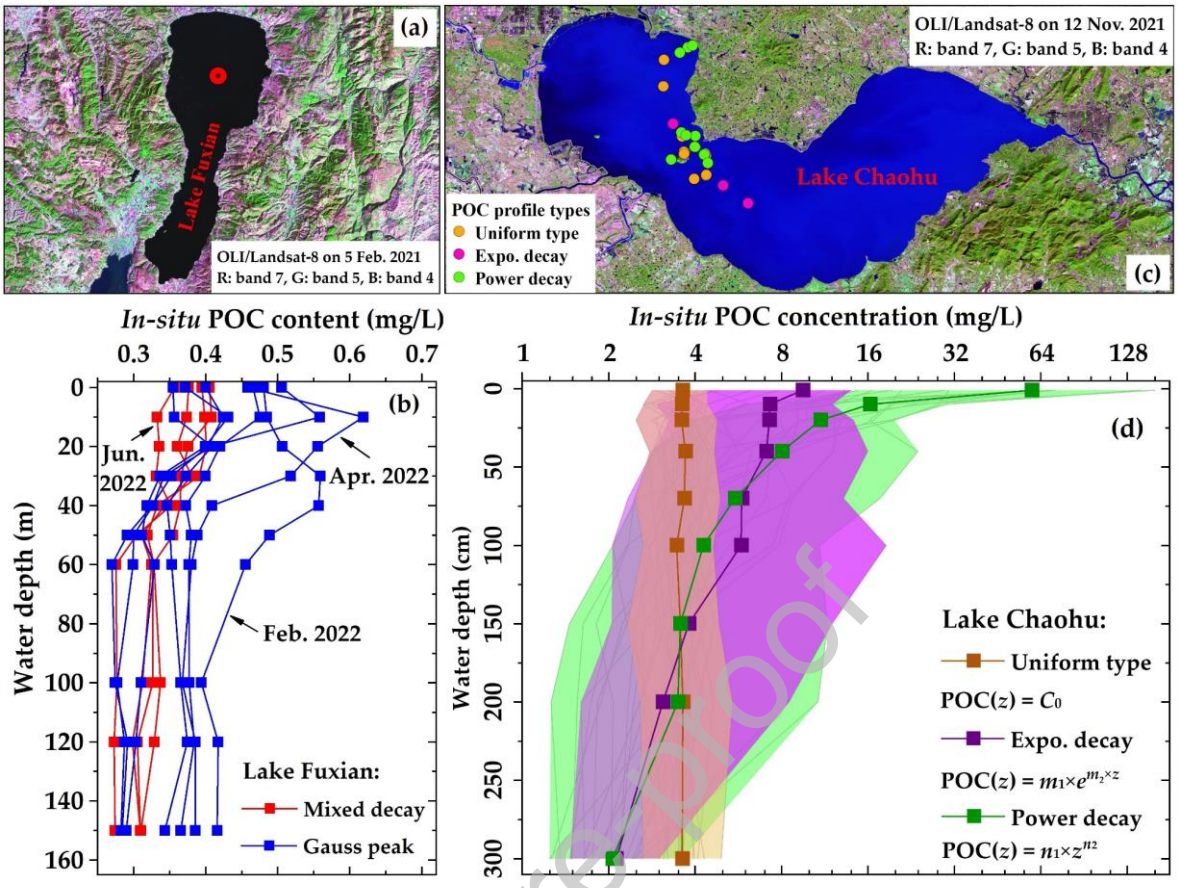

Fig. 12. *In-situ* POC profiles in the typical (a – b) Type-I Lake Fuxian in the YGPL and (c – d) Type-II Lake Chaohu in the EPL (Fig. 1). The colored bands in Fig. 12d show the standard deviations. POC profiles were measured at the stations in Figs. 12a-b (Section 3.1).

Table 1. Statistical information of the sampled lakes. Lake area and DEM were obtained from NIGLAS (2019). Cond.: conductivity; SDD: water transparency indicated by Secchi-disk depth.

No.	Lake name	Area (km^2)	DEM (m)	Longitude (E)	Latitude (N)	Stations	Cond. (μs/cm)	Chl-a (μg/L)	SDD (cm)	POC (mg/L)
1	Ayakkum	616	3876	89°44′	37°29′	4	48548	0.76	140.00	0.45
2	Aibi	565	194	82°59′	44°52′	12	284759	5.25	16.25	3.15
3	Bange	122	4527	89°28′	31°42′	3	47842	3.50	30.00	2.15
4	Bangda	107	4904	81°35′	34°56′	2	28847	0.15	450.00	1.55
5	Bositeng	962	1050	86°59′	41°58′	44	1257	2.04	290.45	0.77
6	Buluntuo	855	478	87°18′	47°16′	24	3441	1.94	148.13	1.07
7	Caizi	71	6	117°9′	30°47′	9	141	49.08	33.89	3.01
8	Chabo	35	4513	84°12′	33°21′	3	120282	0.24	113.33	0.73
9	Chagan	247	126	124°17′	45°15′	19	896	34.31	3.72	4.45
10	Chaohu	787	5	117°31′	31°34′	310	263	56.87	27.85	5.38
11	Cuoe	267	4563	88°48′	31°39′	4	413	0.47	722.50	0.26
12	Daili	214	1223	116°33′	43°18′	3	9527	21.68	3.87	5.33
13	Daihai	87	1218	112°42′	40°34′	10	23428	1.95	240.00	1.30
14	Dianchi	298	1886	102°41′	24°49′	69	430	106.22	36.91	10.03
15	Dongting	144	19	112°57′	29°19′	25	228	8.23	73.60	1.33
16	Eya	57	4822	88°40′	32°59′	8	87994	0.39	214.38	0.31
17	Gasikule	123	2854	90°52′	38°3′	2	105680	0.30	70.00	0.75
18	Gaoyou	703	2	119°13′	32°47′	7	422	28.29	31.23	3.29
19	Gehu	162	0	119°48′	31°35′	11	410	92.35	13.00	6.89
20	Guozha	248	5080	80°56′	35°0′	1	3876	0.07	370.00	0.17
21	Hala	586	4076	97°35′	38°13′	6	16418	0.12	754.00	0.16
22	Hongjian	46	1223	109°53′	39°5′	6	10697	1.41	4.24	0.96
23	Honghu	215	19	113°21′	29°51′	19	342	72.50	32.63	4.86
24	Hongze	1374	10	118°37′	33°18′	172	506	17.55	24.74	2.80
25	Huangda	262	9	116°21′	30°1′	6	277	25.44	31.67	3.30
26	Jili	166	479	87°27′	46°55′	8	1668	2.40	203.75	0.85
27	Jieze	105	4525	80°53′	33°56′	3	90629	0.05	221.67	0.27
28	Keluke	54	2814	96°53′	37°16′	2	990	2.75	330.00	0.60
29	Liangzi	302	16	114°33′	30°14′	20	165	35.72	49.25	3.09
30	Lingge	102	5062	88°37′	33°53′	4	3709	0.31	322.50	0.22
31	Longgan	302	9	116°10′	29°56′	14	278	49.81	27.14	5.05
32	Chaboer	347	4812	81°24′	33°57′	3	17081	1.45	68.33	0.60
33	Luoma	55	17	118°10′	34°5′	9	308	16.65	59.67	1.33
34	Meima	128	4920	82°18′	34°11′	1	9841	0.23	675.00	0.83
35	Nanyi	198	5	118°58′	31°6′	14	174	17.04	31.17	2.53
36	Nvshan	107	11	118°5′	32°58′	3	318	6.67	33.75	1.32
37	Pohu	128	9	116°27′	30°9′	15	180	13.79	54.55	1.88
38	Poyang	2398	10	116°18′	29°12′	25	92	7.09	52.78	1.66
39	Pu'er	39	5048	81°56′	34°53′	4	1213	1.44	98.75	0.63
40	Sailimu	460	2072	81°3′	44°37′	2	3063	0.01	1392.50	0.40
41	Shijiu	214	4	118°55′	31°29′	5	239	5.03	58.60	1.97
42	Songmuxi	25	5051	80°13′	34°36′	3	601	0.57	25.00	0.81
43	Sugan	103	2793	93°55′	38°52′	4	16530	1.03	510.00	0.73
44	Taihu	2329	0	120°9′	31°17′	323	496	38.56	34.21	4.53
45	Tuosu	143	2805	96°53′	37°10′	8	22386	0.61	531.25	0.41

46	Wabu	141	16	116°53′	32°6′	4	251	57.20	29.00	5.23
47	Weishan	175	28	117°15′	34°36'	14	1259	66.33	32.36	6.28
48	Chaidan	62	3173	95°27'	37°28'	1	45188	0.53	4.41	0.32
49	Yibu	65	4557	86°38'	32°51'	1	56605	3.71	105.00	2.03

Table 2 Comparisons of the POC algorithms. $R_{rs}(413)$, $R_{rs}(443)$, $R_{rs}(490)$, $R_{rs}(560)$, $R_{rs}(674)$, $R_{rs}(681)$, and $R_{rs}(708)$ indicate the R_{rs} with central wavelengths of 413, 443, 490, 560, 674, 681, and 708 nm, respectively (Fig. 2b).

No.	The calibrated algorithms	MAPD (%)	RMSE (mg/L)	Bias (%)	References
1	The novel blended algorithm (Eq. (6))	35.93	2.64	-2.73	/
2	Type-I waters ($PH_1 \leq 0.0125$): $\ln(POC) = 1.52 \times R_{rs}(708) / R_{rs}(490) - 0.62$ Type-II waters ($PH_1 > 0.0125$): $\ln(POC) = -1.89 \times R_{rs}(681) / R_{rs}(708) + 3.16$	40.56	2.73	-11.38	Stramski et al., 2008
3	$\ln(POC) = 4.64 \times NDCI + 0.09$ $NDCI = \frac{R_{rs}(560) - \max(R_{rs}(413), R_{rs}(443), R_{rs}(490))}{R_{rs}(560) - \max(R_{rs}(413), R_{rs}(443), R_{rs}(490))}$	66.92	3.71	-20.62	Son et al., 2009
4	$\ln(POC) = 4.64 \times CI + 0.09$ $CI = R_{rs}(560) - (R_{rs}(490) + 0.38 \times (R_{rs}(674) - R_{rs}(490)))$	76.42	3.71	-22.07	Le et al., 2018

Graphical Abstract

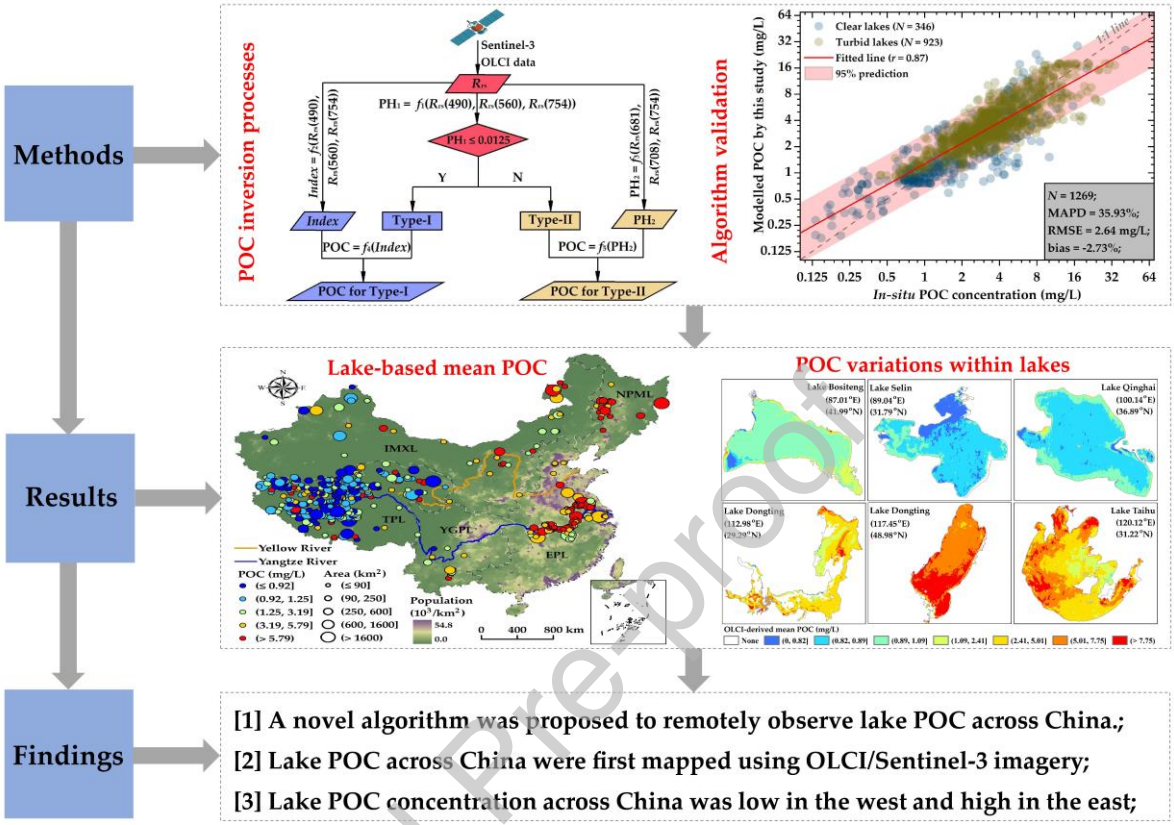

Declaration of interests

☒ The authors declare that they have no known competing financial interests or personal relationships that could have appeared to influence the work reported in this paper.

☐The authors declare the following financial interests/personal relationships which may be considered as potential competing interests: